

# Fixed-phase correlation-function quantum Monte Carlo calculations for ground and excited states of helium in neutron-star magnetic fields

Dirk Meyer, Sebastian Boblest, and Günter Wunner

*Institut für Theoretische Physik 1, Universität Stuttgart, D-70550 Stuttgart, Germany*

(Received 26 November 2012; published 21 March 2013)

We apply the correlation-function quantum Monte Carlo (CFQMC) method to the calculation of the energies of ground and excited states for helium in neutron-star magnetic fields. The method has been successfully applied by Jones, Ortiz, and Ceperley to the calculation of helium in white dwarf magnetic fields [Phys. Rev. E **55**, 6202 (1997)]. We extend the accessible range of magnetic field strengths by introducing a fixed-phase variant of the CFQMC method. We find that with growing magnetic field strength the variances increase significantly and put a limit to the applicability of the method for atoms in strong magnetic fields. The behavior of the variances is traced back to the logarithmic divergence of the energy of the bosonic ground state with increasing magnetic field strength. We use basis sets, which account for the growing dominance of the cylindrical symmetry as the magnetic field is increased and incorporate them into the CFQMC algorithm. These basis sets are taken from Hartree-Fock calculations, performed using a  $B$ -Spline and Landau expansion beyond the adiabatic approximation.

DOI: [10.1103/PhysRevA.87.032515](https://doi.org/10.1103/PhysRevA.87.032515)

PACS number(s): 31.15.vj, 02.70.Tt

## I. INTRODUCTION

Thermal emission of isolated neutron stars with strong cosmic magnetic fields ( $10^6$  to  $10^9$  T) and temperatures of several  $10^5$  K was first observed by the ROSAT satellite in the soft x-ray band (see, e.g., Zampieri *et al.* [1] for the complete list of the sources discovered). More recently, and with higher accuracy, thermal spectra of isolated neutron stars have been measured using the x-ray satellites Chandra and XMM Newton. The observation of features in the x-ray spectra of the neutron-star 1E 1207 has rekindled the interest in the calculation of atomic data of atoms and ions in neutron-star magnetic fields since the observed features could have an atomic origin. The features could provide important information on the chemical composition of the neutron-star surface, the surface gravity from the line broadening, the mass-to-radius ratio from the gravitational redshift of the lines, and the strength of the surface magnetic field.

However, calculations at such huge magnetic field strengths are very hard since the problem of solving the multielectron Schrödinger equation is aggravated by the fact that the magnetic-field effects must be considered nonperturbatively. At neutron-star magnetic field strengths the magnetic field effects are of the same order or even larger than those of the Coulomb field, angular momentum is no longer a good quantum number, and the familiar atomic shell structure has completely collapsed. Different methods have been used in the literature to tackle the problem, ranging from rigorous mathematical estimates over density-functional and discrete-variable methods to different self-consistent field approaches. A comprehensive list of references to work over the past two decades has been given in our paper on quantum Monte Carlo calculations for ground states of medium-heavy atoms in neutron-star magnetic fields [2] (Refs. [1–38] there).

In the present work we adapt the CFQMC method to neutron-star magnetic fields strengths and develop a fixed-phase CFQMC variant to overcome some limitations of the original method. We find that for helium the method is applicable up to a magnetic field strength of  $\beta \approx 40$ , with  $\beta = B/B_0$  and  $B_0 = 4.70103 \times 10^5$  T, thus extending the

range of magnetic field strengths accessible to the CFQMC method by a factor of 10.

The paper is structured as follows. First, in Sec. II we recapitulate the original released-phase CFQMC (RPCFQMC) method and develop the fixed-phase CFQMC (FPCFQMC) method. In Sec. III we describe the trial and guiding functions we used in our calculations. Section IV is devoted to the application of the original and the fixed-phase method to the calculation of ground and excited states of helium in magnetic fields of strengths  $\beta = 0.4$ –40. We compare the results of FPCFQMC to those of RPCFQMC and to results in the literature. Finally, we discuss the reason for the problems occurring when further increasing the magnetic field strength, before we draw conclusions in Sec. V.

## II. CORRELATION-FUNCTION QUANTUM MONTE CARLO METHOD: ESSENTIALS

For the readers' convenience we briefly recapitulate the essential features of the correlation-function quantum Monte Carlo method. A detailed presentation of the method can be found in the original works of Ceperley and Bernu [3] and Jones *et al.* [4].

The aim is to calculate ground and excited states of a many-body Hamiltonian  $\hat{H}$ . For this purpose one chooses a basis of  $m$  linearly independent trial wave functions  $\{f_i(\vec{x})\}$  which are approximations to the lowest  $m$  energy states of the system (the vector  $\vec{x}$  denotes the position vector in the  $3N$  dimensional configuration space of the  $N$  particles). For reasons becoming clear later, a time dependency of the basis is introduced—for the moment it suffices to think of it as being constant at time  $\tau = 0$ .

In the function space spanned by this basis the exact eigenfunctions  $\{|\Psi_i\rangle\}$  of the Hamiltonian can be approximated by the expansion

$$|\tilde{\Psi}_i(\tau)\rangle = \sum_{j=1}^m d_{ij}(\tau) |f_j(\tau)\rangle, \quad (1)$$

with the energies of the approximations  $\{|\tilde{\Psi}_i(\tau)\rangle\}$  given by the Rayleigh coefficients

$$\Lambda_i(\tau) = \frac{\langle \tilde{\Psi}_i(\tau) | \hat{H} | \tilde{\Psi}_i(\tau) \rangle}{\langle \tilde{\Psi}_i(\tau) | \tilde{\Psi}_i(\tau) \rangle}. \quad (2)$$

The expansion coefficients  $d_{ij}(\tau)$  of the approximations of the exact eigenstates are determined by minimizing the Rayleigh coefficients, which leads to a generalized eigenvalue problem

$$\sum_{j=1}^m \mathbf{H}_{kj}(\tau) d_{ij}(\tau) = \Lambda_i(\tau) \sum_{j=1}^m \mathbf{N}_{kj}(\tau) d_{ij}(\tau), \quad (3)$$

with the Hamiltonian matrix  $\mathbf{H}_{kj}(\tau) := \langle f_k(\tau) | \hat{H} | f_j(\tau) \rangle$  and the overlap matrix  $\mathbf{N}_{kj}(\tau) := \langle f_k(\tau) | f_j(\tau) \rangle$ . MacDonald's theorem [5] states that the eigenvalues obtained—the Rayleigh coefficients  $\Lambda_i$ —are upper bounds on the energies of the  $m$  lowest states.

As MacDonald's theorem is valid for *any* basis of  $m$  trial functions, we can improve the basis by evolving it in imaginary time  $\tau$ , thus dampening admixtures of higher energy components relative to the  $m$  lowest energy states

$$|f_i(\tau)\rangle = e^{-\tau \hat{H}/2} |f_i(0)\rangle, \quad (4)$$

with  $\{|f_i(0)\rangle\}$  being the known trial functions. This is similar to the procedure of the diffusion quantum Monte Carlo (DQMC) method and explains the introduction of the (imaginary) time dependence in advance.

To reduce statistical fluctuations in the Monte Carlo evaluation of the  $6N$  dimensional integrals defining the overlap and the Hamiltonian matrix one introduces, as usual, a guiding wave function  $\psi_G$  and the importance sampled trial functions  $F_i = f_i / \psi_G$ . The representation of the matrices in position space

$$\begin{aligned} \mathbf{N}_{kj}(\tau) &= \int d\vec{x} d\vec{x}' F_k^*(\vec{x}') G(\vec{x}', \vec{x}; \tau) F_j(\vec{x}) \psi_G^2(\vec{x}), \\ \mathbf{H}_{kj}(\tau) &= \int d\vec{x} d\vec{x}' F_k^*(\vec{x}') G(\vec{x}', \vec{x}; \tau) E_j(\vec{x}) F_j(\vec{x}) \psi_G^2(\vec{x}) \end{aligned} \quad (5)$$

leads to the importance sampled Green's function

$$G(\vec{x}', \vec{x}; \tau) = \psi_G(\vec{x}') \langle \vec{x}' | e^{-\tau \hat{H}} | \vec{x} \rangle \psi_G^{-1}(\vec{x}) \quad (6)$$

and the local energy of the  $j$ th basis function  $E_j(\vec{x}) = \hat{H} f_j(\vec{x}) / f_j(\vec{x})$ .

The form of the matrices explains the term ‘‘correlation-function quantum Monte Carlo’’ of the approach: Let  $\psi_G^2(\vec{x})$  be the probability that a random walk begins at  $\vec{x}$  and  $G(\vec{x}', \vec{x}; \tau)$  the transition probability that it ends at  $\vec{x}'$  after time  $\tau$ ; then the matrix  $\mathbf{N}_{kj}(\tau)$  can be considered as the autocorrelation function of the vector  $\{F_i(\vec{x})\}$  in time, and  $\mathbf{H}_{kj}(\tau)$  is the correlation between  $F_i(\vec{x})$  and  $E_i(\vec{x}) F_i(\vec{x})$ . The time-difference  $\tau$ , the correlation time, is also called *projection time*.

### A. Released phase CFQMC

As the Green's function of the importance sampled imaginary-time Schrödinger equation (a drift-diffusion equation with a source term and an imaginary paramagnetic

term)

$$\begin{aligned} \frac{\partial f}{\partial \tau} &= \frac{1}{2} \Delta f - \frac{1}{2} \text{div}(f \vec{F}) + \frac{1}{2} f \psi_G^{-1} \Delta \psi_G - (V - E_{\text{Offs}}) f \\ &\quad - \frac{1}{2} \vec{A}^2 f + i \left( \vec{A} \cdot \text{grad} f - \frac{1}{2} f \vec{A} \cdot \vec{F} \right) \end{aligned} \quad (7)$$

is unknown, but the Green's functions of the individual terms are available, a short-time approximation of the Green's function can be obtained according to Trotter's theorem [6] with the partial propagators

$$\begin{aligned} G_d(\vec{x}', \vec{x}; \Delta \tau) &= (2\pi \Delta \tau)^{-3N/2} e^{[\vec{x}' - \vec{x} - \frac{1}{2} \Delta \tau \vec{F}(\vec{x})]^2 / 2\Delta \tau}, \\ G_s(\vec{x}', \vec{x}; \Delta \tau) &= e^{-\Delta \tau \{ [E_L(\vec{x}) + E_L(\vec{x}')]/2 - E_{\text{Offs}} \}}, \\ G_A(\vec{x}', \vec{x}; \Delta \tau) &= e^{-i(\vec{x}' - \vec{x}) \cdot \vec{A} [(\vec{x} + \vec{x}')/2]}, \end{aligned} \quad (8)$$

which account for the drift diffusion, the source term, and the para- and diamagnetic terms, respectively. The local energy of the guiding function  $E_L$  does not have any contributions from the vector potential  $\vec{A}$ , which is accounted for by  $G_A$ , thus

$$E_L(\vec{x}) = \psi_G^{-1} \left[ -\frac{1}{2} \Delta + V(\vec{x}) \right] \psi_G(\vec{x}). \quad (9)$$

The so-called quantum force  $\vec{F}(\vec{x}) = 2\psi_G^{-1}(\vec{x}) \nabla \psi_G(\vec{x})$  enters as the drift and  $E_{\text{Offs}}$  describes an energy offset introduced for convenience. The symmetric gauge of  $\vec{A}$  is used, and  $V$  includes electron-electron, electron-nucleus forces and the spin energies.

The short-time approximation of the Green's function

$$G(\vec{x}', \vec{x}; \tau) \approx \int \dots \int d\vec{x}_1 \dots d\vec{x}_{l-1} \prod_{i=1}^l \tilde{G}(\vec{x}', \vec{x}; \Delta \tau), \quad (10)$$

with

$$\tilde{G}(\vec{x}', \vec{x}; \Delta \tau) = G_d G_s G_A \quad (11)$$

is substituted in (5) and  $G_d$  is interpreted as a transition density generating a random walk.

To obtain a Monte Carlo interpretation and estimators of the matrices one constructs a random walk of length  $l$  along a trajectory  $[\vec{x}_0 = \vec{x}, \vec{x}_1, \dots, \vec{x}_l = \vec{x}']$  according to  $G_d$ , as in the DQMC method, with a time step  $\Delta \tau$  between successive points. Each step of the trajectory is an estimate of one of the integrals over configuration space. Thus the matrices can be estimated as the average over the whole walk

$$\begin{aligned} n_{kj}(p\Delta \tau) &= \frac{1}{2(l-p)} \sum_{n=1}^{l-p} W_{n,n+p} [F_k^*(\vec{x}_n) F_j(\vec{x}_{n+p}) \\ &\quad + F_k^*(\vec{x}_{n+p}) F_j(\vec{x}_n)], \\ h_{kj}(p\Delta \tau) &= \frac{1}{4(l-p)} \sum_{n=1}^{l-p} W_{n,n+p} \\ &\quad \times \{ F_k^*(\vec{x}_n) F_j(\vec{x}_{n+p}) [E_j(\vec{x}_{n+p}) + E_k^*(\vec{x}_n)] \\ &\quad + F_k^*(\vec{x}_{n+p}) F_j(\vec{x}_n) [E_k^*(\vec{x}_{n+p}) + E_j(\vec{x}_n)] \}, \end{aligned} \quad (12)$$

with the complex weights

$$W_{n,n+p} = \prod_{i=n+1}^{n+p} \tilde{G}(\vec{x}_i, \vec{x}_{i-1}; \Delta \tau) / G_d(\vec{x}_i, \vec{x}_{i-1}; \Delta \tau) \quad (13)$$

representing the accumulated weights between points separated by  $p$  time steps on the trajectory. We have used Hermiticity of  $\hat{H}$  to include as much information as available in the estimate.

### B. Fixed-phase CFQMC

It turns out that the partial propagator  $G_A$  increases the noise of the method, which enters in the estimate of the matrices of which eigenvalues are to be determined. To develop a more stable CFQMC variant, the fixed-phase approach of [7] is applied to the CFQMC method, thus making it an approximation, but with the advantage that  $G_A$  is eliminated. By decomposing the wave function into modulus and phase  $\psi(\vec{x}) = |\psi(\vec{x})|\exp[i\varphi_T(\vec{x})]$ , and taking the real part of the imaginary-time Schrödinger equation, one arrives at the fixed-phase equation for the modulus of the wave function

$$\left\{ -\frac{1}{2}\Delta + \frac{1}{2}[\nabla\varphi_T(\vec{x}) + \vec{A}(\vec{x})]^2 + V(\vec{x}) - E_{\text{offs}} \right\} |\psi| = E|\psi|, \quad (14)$$

with the fixed trial phase function  $\varphi_T(\vec{x})$ . Introducing importance sampling and simulating this equation one finds the lowest energy for a given trial phase [7]. The term in brackets defines the fixed-phase Hamiltonian  $\hat{H}_{\text{FP}}$ . Local energy is calculated using the fixed-phase Hamiltonian with respect to the modulus of the wave function

$$E_L = \frac{\hat{H}_{\text{FP}}|\psi|}{|\psi|} = \text{Re} \frac{\hat{H}[|\psi|\exp(i\varphi_T)]}{|\psi|\exp(i\varphi_T)}. \quad (15)$$

Because the imaginary paramagnetic term does not appear in (14) and is implicitly accounted for by the choice of the trial phase, the partial propagator  $G_A$  is dropped from the propagators (8), while  $G_d$  and  $G_s$  are retained. The vector potential  $\vec{A}$  has the form of a source term and is taken into account by  $G_s$  with the local energy as defined in (15).

### III. CHOICE OF THE TRIAL AND GUIDING FUNCTIONS

We use basis states in a Landau expansion adapted to strong magnetic fields of neutron stars. The basis functions  $f_k$  are Slater determinants with single particle orbitals of the form

$$\psi(\rho, \varphi, z) = \sum_{n=0}^{N_L} P_n(z) \Phi_n(\rho, \varphi), \quad (16)$$

where for any magnetic field strength the  $z$ -dependent expansion coefficients  $P_{in}$  are determined using self-consistent 2D Hartree-Fock-Roothaan (2DHFR) calculations. This ansatz is complete for a given symmetry subspace with the only drawback being the truncation to a maximum of  $N_L + 1 = 31$  Landau functions  $\Phi_n$ . This ansatz is an improvement on the ansatz presented in [8] and on the ansatz used in the DQMC calculations for ground states of the elements up to neutral iron in strong magnetic fields [2]. Because of the high spin-flip energy of  $2\beta$ , the electron spins are all aligned antiparallel to the magnetic field direction and the spin degree of freedom can completely be accounted for by an energy shift incorporated into the potential  $V$ . In the limit of infinite magnetic field strength, the exact solution just includes the zeroth Landau function (this is called adiabatic approximation for high, but

finite field strengths), therefore this ansatz is particularly well suited for high magnetic field strengths.

For the walks to be capable of sampling all relevant ranges of position space, the guiding function has to reflect the ground state plus all excited states to be calculated. The guiding function has to be real to avoid phase cancellation between different states. To lower variance, the guiding function must not have any nodes the walk could encounter, otherwise the term  $f_i/\psi_G$  in the estimates of the matrices would diverge. We use a slightly modified version of the guiding function of Jones *et al.* [4]

$$\psi_G(\vec{x}) = C \left[ \frac{c_0}{m} \sum_{i=1}^m \prod_{j=1}^N \rho_i(\vec{x}_j) + \sum_{i=1}^m c_i |f_i(\vec{x})|^2 \right]^{\frac{1}{2}}, \quad (17)$$

which includes the single state electron density

$$\rho_i(\vec{x}_j) = \sum_{k=1}^N |\psi_{i,k}(\vec{x}_j)|^2 \quad (18)$$

to make the guiding function node-free. In (18)  $\psi_{i,k}$  is the  $k$ th single state wave function given in (16) forming the Slater determinant of the  $i$ th trial function. The trial functions and single state wave functions are normalized, and the constant

$$C = \left( c_0 N^N + \sum_{i=1}^m c_i \right)^{-\frac{1}{2}} \quad (19)$$

takes care of the normalization of the guiding function. The remaining constants  $c_0$  and  $c_i$  are adjusted by hand to modify the amount of overlap with any given state and thus to balance the variance of the results for the corresponding states. In agreement with [9] we obtained best results if  $c_0$  was chosen such that for approximately 10% of configurations the first term in (17) yields a larger value than the second.

### IV. APPLICATION TO NEUTRAL He ATOMS IN STRONG MAGNETIC FIELDS

We employed ensemble sizes of typically a few thousand walkers, each of which was used at each projection time to (a) sum up a global estimate of the  $\mathbf{H}$  and  $\mathbf{N}$  matrices, and (b) to estimate the eigenvalues for each walk separately. The eigenvalues  $\lambda(\tau)$  of the summed-up matrices in step (a) are shown in the figures. The bias entering the method because of the nonlinear process of finding eigenvalues was at least two orders of magnitude smaller than the standard deviation. The separately estimated eigenvalues  $\bar{\lambda}_i(\tau)$  in step (b) were used to estimate the standard deviation. We estimated the bias  $b(\tau)$  for each state and each projection time with the general relation [3]

$$b(\tau) = \left[ \sum_{i=1}^{N_w} \bar{\lambda}_i(\tau)/N_w - \lambda(\tau) \right] / (N_w - 1) \quad (20)$$

as the deviation of the average of the eigenvalues of  $N_w$  successful walks from the eigenvalues of the summed-up matrices. ‘‘Successful’’ means that only walks leading to a positive definite overlap matrix for the considered projection time can be taken into account. Only the matrices of successful walks were used in the summed-up matrices.

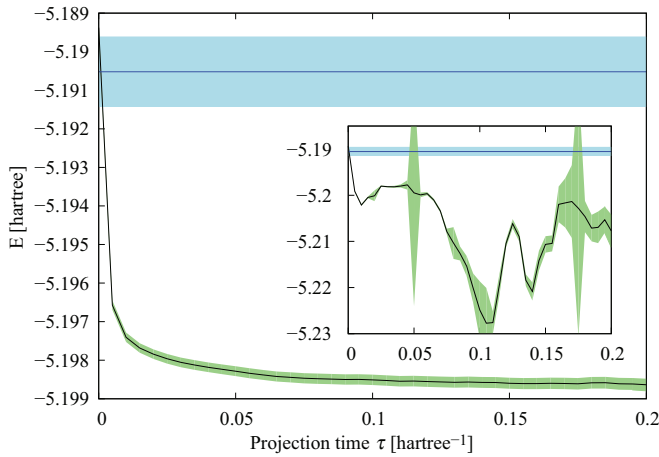


FIG. 1. (Color online) Fixed-phase and released-phase (inset) correlation-function quantum Monte Carlo calculation for the second excited state of the  $(\pi_z = +, L_z = -1)$  symmetry subspace of neutral helium in a magnetic field of strength  $\beta = 8$ . In this range the variance is too high for the released-phase method to gain results. See the text for an interpretation of the released-phase result. The fixed-phase calculation has the same parameters and the same sequence of random numbers as the released-phase (inset). The statistical noise is significantly lower, one notes a fast relaxation to the true energy, which thus can be obtained successfully. The black line is the eigenvalue corresponding to the state, estimated at projection times each  $0.005 \text{ hartree}^{-1}$ . The green area marks the estimated  $\pm 1\sigma$  area. The horizontal blue line is the variational quantum Monte Carlo energy of the two-dimensional Hartree-Fock-Roothaan trial function the correlation-function quantum Monte Carlo method starts from within its  $\pm 1\sigma$  area of confidence. The calculation was carried out with 12 million correlation-function quantum Monte Carlo steps per walker with  $\Delta\tau = 10^{-4} \text{ hartree}^{-1}$ , an equilibration of 800 000 VQMC steps per walker, an ensemble of 2560 walkers and the  $c$  parameters for the guiding function being  $\{0.2, 1.5, 2.25, 3.375\}$ . Estimates of the eigenvalues have been generated every  $0.005 \text{ hartree}^{-1}$ , the line serves as a guide to the eye.

Compared to the DQMC method much longer walks were needed to equilibrate the ensemble to a stochastic representation of the guiding function, because it is composed of trial functions of quite different spatial extents. The ensemble has to reflect small structures of the ground state and at the same time has to cover the whole space occupied by the highest excited state. Comparison of the CFQMC result at zero projection time with the VQMC energy of the trial function is a measure for the quality of equilibration. It was also necessary to drastically increase the number of steps in the CFQMC calculations compared to DQMC calculations to avoid unsuccessful walks which result in unusable nonpositive definite estimates of the overlap matrix because of high statistical noise.

### A. RPCFQMC and FPCFQMC results

We carried out calculations with the RPCFQMC method and were able to reproduce the results of Jones *et al.* [4], but it was not possible to extend the range of magnetic field strengths above the range considered by Jones *et al.* In particular, it was not possible to gain meaningful results for helium above  $\beta_Z \approx 1$  with few exceptions in the case  $L_z = 0$ , though our trial

functions are known to become more and more accurate the higher the magnetic field strength is. For the lowest magnetic field strengths accessible with our trial functions  $\beta_Z = 0.1$ , the RPCFQMC method yields good results, but variance increases with increasing magnetic fields, until it becomes so high that the method is not capable of producing convergence at  $\beta_Z \geq 1$ .

An example is depicted in the inset of Fig. 1 for  $\beta_Z = 2$ . The eigenvalues do not show any convergence to the resulting energy, the obviously wrong estimate of the standard deviation is a sign that only a few walkers from the same limited configuration space volume are contributing to the result, while the estimates of the overlap matrices of the other walkers are not positive definite because of statistical noise. The peaks in standard deviation signal a walker for which the overlap matrix becomes nonpositive definite after some projection time. Shortly before this happens, the estimated eigenvalue of the affected walker shows high fluctuations and destroys the estimate of the standard deviation. Afterwards, it is ignored completely.

The same calculation using the fixed-phase CFQMC method is shown in Fig. 1. We chose the phase of the highest excited 2DHFR trial function of each calculation as our trial phase, because this state is the one with the largest spatial extent. The noise is reduced by a large amount, and with the FPCFQMC method it is possible to extend the range of accessible magnetic field strengths to  $\beta \approx 40$ . Comparison of the results with the RPCFQMC method shows agreement in the range accessible to both methods within statistical error. This means that the trial phase is exact within the statistical limit. To test the greater stability of the fixed-phase method compared to the released phase, we plotted intermediate results of a calculation to examine the convergence properties of the methods. Figure 2 shows an example. Clearly the FPCFQMC

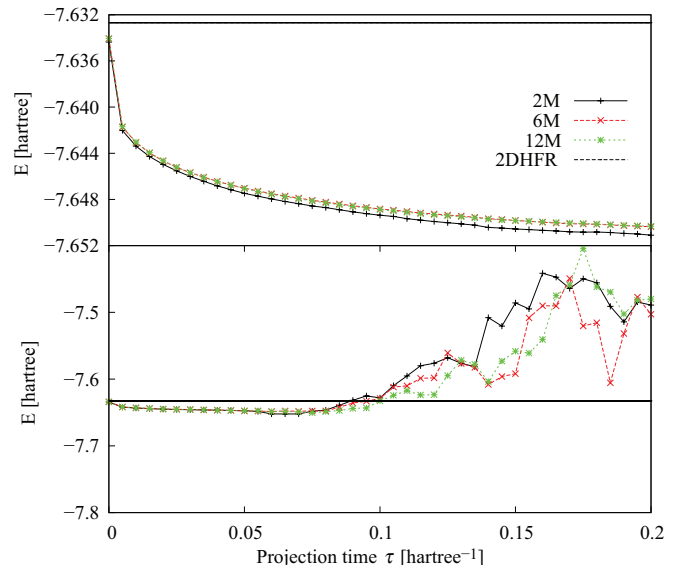


FIG. 2. (Color online) Convergence properties of the fixed-phase correlation-function quantum Monte Carlo method (top) compared with the released-phase method (bottom). The figure shows a calculation for the ground state of the  $(\pi_z = -, L_z = 0)$  symmetry subspace for neutral helium at  $\beta = 21.27$ . Intermediate results taken at 2 million steps, 6 million steps, and 12 million steps are shown. The horizontal line is the variational quantum Monte Carlo result of the two-dimensional Hartree-Fock-Roothaan trial function used.

TABLE I. CFQMC energies ( $-E_{\text{CFQMC}}$ ) of helium of the ( $\pi_z = +, L_z = -1$ ) subspace in Hartree with  $1\sigma$  standard deviations in relation to the last given digit in parentheses. The last three columns show VQMC energies of the Hartree-Fock trial functions we used. The electron configuration of each state is given by its field-free quantum numbers and the  $(-m, \nu)$  quantum numbers. Note that computational effort was increased for  $\beta \geq 8$ .

| $\beta$ | FPCFQMC             |                     |                     | RPCFQMC             |                     |                     | 2DHFR               |                     |                     |
|---------|---------------------|---------------------|---------------------|---------------------|---------------------|---------------------|---------------------|---------------------|---------------------|
|         | $1s2p_{-1}$<br>0010 | $1s3p_{-1}$<br>0012 | $1s4p_{-1}$<br>0014 | $1s2p_{-1}$<br>0010 | $1s3p_{-1}$<br>0012 | $1s4p_{-1}$<br>0014 | $1s2p_{-1}$<br>0010 | $1s3p_{-1}$<br>0012 | $1s4p_{-1}$<br>0014 |
| 0.4     | 2.833(3)            | 2.483(1)            | 2.412(1)            | 2.827(2)            | 2.481(1)            | 2.413(1)            | 2.7599(7)           | 2.4159(6)           | 2.3474(6)           |
| 0.8     | 3.309(2)            | 2.8003(8)           | 2.7179(9)           | 3.304(2)            | 2.8000(8)           | 2.717(1)            | 3.2670(6)           | 2.7663(5)           | 2.6854(5)           |
| 1.2     | 3.693(2)            | 3.0636(8)           | 2.9731(7)           | 3.687(2)            | 3.0631(8)           | 2.9733(9)           | 3.6567(6)           | 3.0384(5)           | 2.9488(5)           |
| 2.0     | 4.309(2)            | 3.4915(7)           | 3.3913(8)           | 4.303(2)            | 3.4903(6)           | 3.3906(7)           | 4.2798(7)           | 3.4746(5)           | 3.3738(5)           |
| 2.8     | 4.806(2)            | 3.8413(7)           | 3.7333(7)           | 4.798(2)            | 3.8419(8)           | 3.7335(7)           | 4.7741(6)           | 3.8265(5)           | 3.7210(5)           |
| 4.0     | 5.416(2)            | 4.2750(6)           | 4.1602(7)           | 5.407(3)            | 4.2739(6)           | 4.1603(6)           | 5.3856(6)           | 4.2629(6)           | 4.1479(5)           |
| 8.0     | 6.8820(4)           | 5.3268(2)           | 5.1986(2)           |                     |                     |                     | 6.8554(8)           | 5.3166(8)           | 5.1902(6)           |
| 20.0    | 9.5019(8)           | 7.2152(2)           | 7.0719(2)           |                     |                     |                     | 9.475(2)            | 7.206(2)            | 7.063(1)            |
| 21.27   | 9.7088(4)           | 7.3652(2)           | 7.2212(2)           |                     |                     |                     | 9.686(2)            | 7.360(2)            | 7.217(2)            |
| 28.0    | 10.6913(7)          | 8.0764(2)           | 7.9271(2)           |                     |                     |                     | 10.670(2)           | 8.068(2)            | 7.918(1)            |
| 40.0    | 12.1056(3)          | 9.1010(2)           | 8.9456(2)           |                     |                     |                     | 12.092(3)           | 9.095(2)            | 8.941(2)            |

method does not only show a converged result over the whole projection time, but also the convergence to this result is steady. The RPCFQMC methods shows nearly random behavior for  $\tau > 0.1$ .

The comparison of fixed-phase with released-phase CFQMC results (see Tables I–IV) reveals overlap of the  $1\sigma$  range for all results except the ground state of the  $(+, -1)$  symmetry subspace, for which one finds overlap of the  $2\sigma$  ranges only, and two results from the  $(-, 0)$  subspace. The subspaces with  $L_z = 0$  often show identical results for all digits given, which can be expected, because the trial functions are real and the complications arising from  $G_A$  (which nevertheless is still present in the released-phase variant) can be considered less severe.

However, the general behavior of the CFQMC method, that variance increases with increasing magnetic field strength, remains unchanged. We assume that the reason for this behavior is that the variance  $\sigma_k^2$  is governed by the exponential of the energy difference between the state  $k$  in question and the bosonic ground state [3]

$$\lim_{p \rightarrow \infty} \sigma_k^2(p\Delta\tau) \geq \frac{1}{l-p} C_k e^{2p\Delta\tau(E_k - E_0)}. \quad (21)$$

The bosonic ground state is the absolute ground state of the considered Hamiltonian and is symmetric under particle exchange.

The bosonic ground state (or in general, the state with the lowest energy) enters the variance because of the long-time limit of the Green's function

$$\lim_{\tau \rightarrow \infty} G(\vec{x}', \vec{x}; \tau) = \frac{\psi_G(\vec{x}')}{\psi_G(\vec{x})} e^{-\tau(E_0 - E_{\text{offs}})} \Psi_0(\vec{x}') \Psi_0^*(\vec{x}), \quad (22)$$

which is taken into account by the weights. The bosonic ground state is denoted as  $\Psi_0$  and its energy  $E_0$ . One can derive this spectral decomposition by starting from (6) and inserting the spectrum of the Hamiltonian twice. In the imaginary-time evolution, the bosonic ground state decays slowest.

In our application one obtains the bosonic ground state by putting both electrons into the lowest single-particle hydrogen

orbital with same spin. The fermionic ground state is the first excited state of the Hamiltonian, as one electron has to be lifted to the first excited single particle hydrogen state to conform to the Pauli principle for fermions. Both states are tightly bound and their energies diverge logarithmically in the limit of infinite magnetic field strength, but with a different prefactor. The energy difference between the fermionic and bosonic ground state increases proportional to  $\sqrt{\beta}$  as can be seen in Fig. 3. For excited states within a symmetry subspace, one electron has to be lifted to a hydrogenlike state, with an energy converging to a constant value in the limit of infinite magnetic field strength, therefore the energy difference increases even faster.

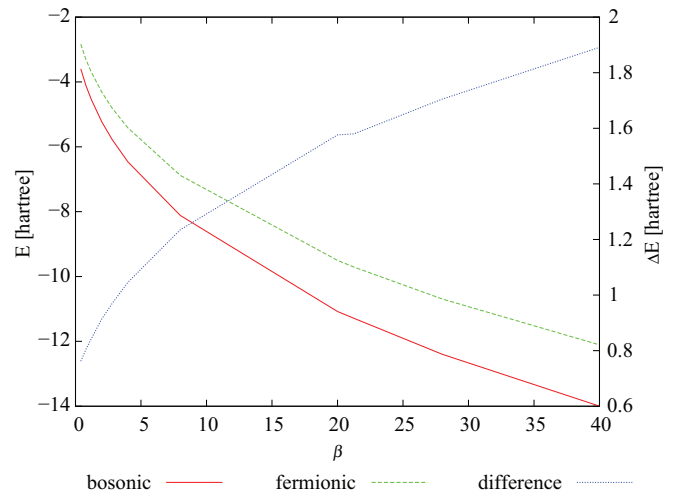


FIG. 3. (Color online) Energies of the bosonic (absolute) and the fermionic ground state over increasing magnetic field strength. The bosonic ground state has the (field-free) electronic configuration  $1s^2$ , the fermionic  $1s2p_{-1}$ , which is the ground state of helium for the displayed range of magnetic field strength. One easily sees the increasing difference proportional to  $\sqrt{\beta}$ , which poses a problem on the CFQMC method, as this energy difference increases variance. For excited fermionic states, energy difference is even larger. Results for individual magnetic field strengths were calculated using DQMC, the lines serve as guides to the eye.

TABLE II. CFQMC energies ( $-E_{\text{CFQMC}}$ ) of helium of the ( $\pi_z = -, L_z = -1$ ) subspace in Hartree with  $1\sigma$  standard deviations in relation to the last given digit in parentheses. A  $<$  sign marks cases in which the calculation was not converged fully, so only an upper limit was obtained. The last three columns show VQMC energies of the Hartree-Fock trial functions we used. The electron configuration of each state is given by its field-free quantum numbers and the  $(-m, \nu)$  quantum numbers. Note that computational effort was increased for  $\beta \geq 8$ .

| $\beta$ | FPCFQMC             |                     |                     | RPCFQMC             |                     |                     | 2DHFR               |                     |                     |
|---------|---------------------|---------------------|---------------------|---------------------|---------------------|---------------------|---------------------|---------------------|---------------------|
|         | $1s3d_{-1}$<br>0011 | $1s4d_{-1}$<br>0013 | $1s5d_{-1}$<br>0015 | $1s3d_{-1}$<br>0011 | $1s4d_{-1}$<br>0013 | $1s5d_{-1}$<br>0015 | $1s3d_{-1}$<br>0011 | $1s4d_{-1}$<br>0013 | $1s5d_{-1}$<br>0015 |
| 0.4     | 2.555(2)            | 2.4324(8)           | 2.396(2)            | 2.553(2)            | 2.4332(8)           | 2.396(3)            | 2.4863(8)           | 2.3682(6)           | 2.3322(6)           |
| 0.8     | 2.89(1)             | 2.74(1)             | 2.70(1)             | 2.894(2)            | 2.7424(7)           | 2.700(3)            | 2.8596(7)           | 2.7094(5)           | 2.6674(5)           |
| 1.2     | 3.171(2)            | 2.9987(7)           | 2.954(1)            | 3.170(2)            | 2.9996(7)           | 2.954(2)            | 3.1445(6)           | 2.9758(6)           | 2.9283(5)           |
| 2.0     | 3.618(2)            | 3.4187(7)           | 3.3703(8)           | 3.616(2)            | 3.4191(8)           | 3.370(1)            | 3.5993(7)           | 3.4035(6)           | 3.3550(5)           |
| 2.8     | 3.978(2)            | 3.7632(7)           | 3.7119(9)           | 3.976(2)            | 3.7642(8)           | 3.712(1)            | 3.9625(7)           | 3.7499(6)           | 3.6994(5)           |
| 4.0     | 4.423(2)            | 4.1908(7)           | 4.137(1)            | <4.419(2)           | 4.1912(7)           | 4.137(1)            | 4.4086(7)           | 4.1797(6)           | 4.1263(6)           |
| 8.0     | 5.4880(5)           | 5.2306(2)           | 5.1736(2)           |                     |                     |                     | 5.478(2)            | 5.2206(9)           | 5.1631(8)           |
| 20.0    | <7.3922(2)          | 7.1041(2)           | 7.0432(1)           |                     |                     |                     | 7.382(2)            | 7.098(2)            | 7.037(2)            |
| 21.27   | <7.5437(4)          | 7.2538(4)           | 7.1927(3)           |                     |                     |                     | 7.534(2)            | 7.244(2)            | 7.185(1)            |
| 28.0    |                     |                     |                     |                     |                     |                     | 8.245(2)            | 7.950(2)            | 7.890(2)            |
| 40.0    |                     | 8.9770(2)           | 8.9146(3)           |                     |                     |                     | 9.272(2)            | 8.968(2)            | 8.909(2)            |

TABLE III. CFQMC energies ( $-E_{\text{CFQMC}}$ ) of helium of the ( $\pi_z = +, L_z = 0$ ) subspace in Hartree with  $1\sigma$  standard deviations in relation to the last given digit in parentheses. The last three columns show VQMC energies of the Hartree-Fock trial functions we used. The electron configuration of each state is given by its field-free quantum numbers and the  $(-m, \nu)$  quantum numbers. Note that computational effort was increased for  $\beta \geq 8$ .

| $\beta$ | FPCFQMC        |                |                | RPCFQMC        |                |                | 2DHFR          |                |                |
|---------|----------------|----------------|----------------|----------------|----------------|----------------|----------------|----------------|----------------|
|         | $1s2s$<br>0002 | $1s3s$<br>0004 | $1s4s$<br>0006 | $1s2s$<br>0002 | $1s3s$<br>0004 | $1s4s$<br>0006 | $1s2s$<br>0002 | $1s3s$<br>0004 | $1s4s$<br>0006 |
| 0.4     | 2.569(2)       | 2.4385(9)      | 2.398(5)       | 2.569(2)       | 2.4381(8)      | 2.397(6)       | 2.497(1)       | 2.3705(7)      | 2.3325(7)      |
| 0.8     | 2.865(2)       | 2.7337(7)      | 2.697(3)       | 2.865(2)       | 2.7337(7)      | 2.695(6)       | 2.8283(8)      | 2.7006(6)      | 2.6649(6)      |
| 1.2     | 3.120(2)       | 2.9866(7)      | 2.948(4)       | 3.120(2)       | 2.9866(7)      | 2.948(6)       | 3.095(2)       | 2.9603(6)      | 2.9234(6)      |
| 2.0     | 3.544(2)       | 3.4039(6)      | 3.365(4)       | 3.544(2)       | 3.4040(6)      | 3.364(5)       | 3.5240(7)      | 3.3859(6)      | 3.3473(5)      |
| 2.8     | 3.890(1)       | 3.7454(6)      | 3.705(4)       | 3.889(2)       | 3.7454(6)      | 3.705(5)       | 3.8732(9)      | 3.7304(6)      | 3.6920(6)      |
| 4.0     | 4.321(2)       | 4.1709(6)      | 4.130(2)       | 4.321(2)       | 4.1708(6)      | 4.129(2)       | 4.3066(7)      | 4.1574(7)      | 4.1170(6)      |
| 8.0     | 5.3690(3)      | 5.2081(2)      | 5.1658(2)      | 5.3684(4)      | 5.2077(3)      | 5.1661(4)      | 5.358(2)       | 5.198(1)       | 5.156(1)       |
| 20.0    | 7.2556(2)      | 7.0799(1)      | 7.0352(1)      |                |                |                | 7.248(2)       | 7.074(2)       | 7.025(1)       |
| 21.27   | 7.4059(3)      | 7.2294(2)      | 7.1844(3)      | 7.4049(6)      | 7.2291(5)      | 7.1841(4)      | 7.397(2)       | 7.224(2)       | 7.178(2)       |
| 28.0    | 8.1166(3)      | 7.9350(1)      | 7.88944(9)     |                |                |                | 8.104(2)       | 7.924(2)       | 7.883(2)       |
| 40.0    | 9.1399(2)      | 8.95312(9)     | 8.90662(8)     |                |                |                | 9.131(2)       | 8.943(2)       | 8.897(2)       |

TABLE IV. CFQMC energies ( $-E_{\text{CFQMC}}$ ) of helium of the ( $\pi_z = -, L_z = 0$ ) subspace in Hartree with  $1\sigma$  standard deviations in relation to the last given digit in parentheses. The last three columns show VQMC energies of the Hartree-Fock trial functions we used. The electron configuration of each state is given by its field-free quantum numbers and the  $(-m, \nu)$  quantum numbers. Note that computational effort was increased for  $\beta \geq 8$ .

| $\beta$ | FPCFQMC          |                  |                  | RPCFQMC          |                  |                  | 2DHFR            |                  |                  |
|---------|------------------|------------------|------------------|------------------|------------------|------------------|------------------|------------------|------------------|
|         | $1s2p_0$<br>0001 | $1s3p_0$<br>0003 | $1s4p_0$<br>0005 | $1s2p_0$<br>0001 | $1s3p_0$<br>0003 | $1s4p_0$<br>0005 | $1s2p_0$<br>0001 | $1s3p_0$<br>0003 | $1s4p_0$<br>0005 |
| 0.4     | 2.631(3)         | 2.4508(9)        | 2.402(3)         | 2.631(2)         | 2.4508(9)        | 2.402(3)         | 2.5651(7)        | 2.3862(7)        | 2.3396(6)        |
| 0.8     | 2.983(2)         | 2.7584(9)        | 2.705(2)         | 2.984(2)         | 2.7584(8)        | 2.705(2)         | 2.9474(6)        | 2.7251(6)        | 2.6726(5)        |
| 1.2     | 3.266(2)         | 3.0148(7)        | 2.959(3)         | 3.263(2)         | 3.0149(7)        | 2.958(3)         | 3.2404(6)        | 2.9903(5)        | 2.9336(5)        |
| 2.0     | 3.722(2)         | 3.4358(7)        | 3.376(3)         | 3.722(2)         | 3.4358(7)        | 3.376(3)         | 3.7011(7)        | 3.4194(5)        | 3.3591(6)        |
| 2.8     | 4.086(2)         | 3.7793(7)        | 3.717(2)         | 4.086(2)         | 3.7793(8)        | 3.717(2)         | 4.0640(7)        | 3.7627(6)        | 3.7037(6)        |
| 4.0     | 4.533(3)         | 4.2060(9)        | 4.142(3)         | 4.532(2)         | 4.2055(8)        | 4.142(2)         | 4.5135(6)        | 4.1932(6)        | 4.1303(6)        |
| 8.0     | 5.6034(4)        | 5.2456(2)        | 5.1781(2)        | 5.5994(4)        | 5.2466(8)        | 5.1775(2)        | 5.586(1)         | 5.235(1)         | 5.1674(9)        |
| 20.0    | 7.4999(2)        | 7.11741(9)       | 7.04725(8)       |                  |                  |                  | 7.483(2)         | 7.109(2)         | 7.038(1)         |
| 21.27   | 7.6503(3)        | 7.2666(2)        | 7.1964(2)        | 7.649(1)         | 7.2674(6)        | 7.1963(6)        | 7.633(2)         | 7.258(2)         | 7.193(2)         |
| 28.0    |                  | 7.97174(9)       | 7.90115(8)       |                  |                  |                  | 8.343(2)         | 7.965(2)         | 7.892(2)         |
| 40.0    | 9.3796(2)        | 8.98927(9)       | 8.91805(8)       |                  |                  |                  | 9.366(2)         | 8.977(2)         | 8.909(2)         |

TABLE V. Comparison of our results for the states  $1s2p_{-1}$ ,  $1s3p_{-1}$ , and  $1s4p_{-1}$  with work of other groups.

| $\beta$ | $1s2p_{-1}$ |           |               | $1s3p_{-1}$ |           | $1s4p_{-1}$ |           |
|---------|-------------|-----------|---------------|-------------|-----------|-------------|-----------|
|         | FPCFQMC     | Ref. [10] | Ref. [11]     | FPCFQMC     | Ref. [10] | FPCFQMC     | Ref. [10] |
| 0.4     | 2.833(3)    | 2.8301    | 2.8378(0)     | 2.483(1)    | 2.4855    | 2.412(1)    | 2.4178    |
| 0.8     | 3.309(2)    | 3.3016    | 3.3170(6)     | 2.8003(8)   | 2.8006    | 2.7179(9)   | 2.7188    |
| 1.2     | 3.693(2)    | 3.6842    |               | 3.0636(8)   | 3.0630    | 2.9731(7)   | 2.9735    |
| 2.0     | 4.309(2)    | 4.2980    | 4.3100(44)    | 3.4915(7)   | 3.4903    | 3.3913(8)   | 3.3909    |
| 2.8     | 4.806(2)    | 4.7911    | 4.8058(26)    | 3.8413(7)   | 3.8411    | 3.7333(7)   | 3.7343    |
| 4.0     | 5.416(2)    | 5.4000    | 5.4052(64)    | 4.2750(6)   | 4.2742    | 4.1602(7)   | 4.1605    |
| 8.0     | 6.8820(4)   | 6.8666    | 6.8768(150)   | 5.3268(2)   | 5.3261    | 5.1986(2)   | 5.1995    |
| 20.0    | 9.5019(8)   | 9.4882    | 9.5004(628)   | 7.2152(2)   | 7.2156    | 7.0719(2)   | 7.0714    |
| 28.0    | 10.6913(7)  | 10.6816   | 10.6948(1112) | 8.0764(2)   | 8.0768    | 7.9271(2)   | 7.9268    |
| 40.0    | 12.1065(3)  | 12.1011   | 12.1086(1582) | 9.1010(2)   | 9.1010    | 8.9456(2)   | 8.9451    |

### B. Comparison with other calculations

Table V lists comparisons of our results for the states  $1s2p_{-1}$ ,  $1s3p_{-1}$ , and  $1s4p_{-1}$  with results obtained in a Hartree-Fock approach by Jones *et al.* [10]. Recently, Thirumalai and Heyl [11] presented results for some helium states including  $1s2p_{-1}$  obtained using a two-dimensional Hartree-Fock method that is especially accurate for small magnetic field strengths. We present the results of this study as an additional reference value.

Our results are of comparable or higher accuracy except for the lowest field strengths. The decreasing accuracy there can be explained by the truncation error in the single particle orbitals used in our trial functions, which grows rather large for  $\beta_Z \ll 1$ . However, we are able to reach much higher accuracies in conventional FPDQMC calculations for ground state energies using these trial functions, as we will show in a forthcoming publication.

Our results for the states presented in Tables II–IV show a similar performance when compared to the studies [10] and [11].

### V. CONCLUSIONS

We developed the fixed-phase variant of the CFQMC method and found it to be much more robust than the original released-phase CFQMC method, while being equally

exact in our application. The advantage of the FPCFQMC method compared to the FPDQMC method is that the former is variational also for excited states. In the FPCFQMC method, the dependence of the variance on the energy difference between the energy of the calculated state and the absolute ground state remains unchanged, which means that the method is applicable to cases in which this energy difference is small. The increasing quality of our trial functions for higher magnetic field strengths cannot compensate for the growth of the variance. The FPCFQMC method allowed for the calculation of energies of excited states for helium in neutron-star magnetic fields up to a magnetic field strength of approximately  $\beta = 40$ . As the energy difference between the bosonic and fermionic ground state for higher elements increases compared to helium, we do not expect the method to be suitable in these cases. The self-healing DQMC algorithms recently extended to excited states and magnetic fields [12,13] seem promising to tackle this problem, with the increased expense of even longer calculation times.

### ACKNOWLEDGMENTS

We thank C. Schimeczek for providing his Hartree-Fock results. This work was supported by Deutsche Forschungsgemeinschaft. We gratefully thank the bwGRiD project [14] for the computational resources.

- 
- [1] L. Zampieri, S. Campana, R. Turolla, M. Chierigato, R. Falomo, D. Fugazza, A. Moretti, and A. Treves, *Astron. Astrophys.* **378**, L5 (2001).
- [2] S. Bücheler, D. Engel, J. Main, and G. Wunner, *Phys. Rev. A* **76**, 032501 (2007).
- [3] D. M. Ceperley and B. Bernu, *J. Chem. Phys.* **89**, 6316 (1988).
- [4] M. D. Jones, G. Ortiz, and D. M. Ceperley, *Phys. Rev. E* **55**, 6202 (1997).
- [5] J. K. L. MacDonald, *Phys. Rev.* **43**, 830 (1933).
- [6] H. F. Trotter, *Proc. Am. Math. Soc.* **10**, 545 (1959).
- [7] G. Ortiz, D. M. Ceperley, and R. M. Martin, *Phys. Rev. Lett.* **71**, 2777 (1993).
- [8] D. Engel and G. Wunner, *Phys. Rev. A* **78**, 032515 (2008).
- [9] D. M. Ceperley and B. J. Alder, *J. Chem. Phys.* **81**, 5833 (1984).
- [10] M. D. Jones, G. Ortiz, and D. M. Ceperley, *Phys. Rev. A* **59**, 2875 (1999).
- [11] A. Thirumalai and J. S. Heyl, *Phys. Rev. A* **79**, 012514 (2009).
- [12] F. A. Reboredo, *Phys. Rev. B* **80**, 125110 (2009).
- [13] F. A. Reboredo, *J. Chem. Phys.* **136**, 204101 (2012).
- [14] bwGRiD (<http://www.bw-grid.de/>), Member of the German D-Grid initiative, funded by the Ministry of Education and Research (Bundesministerium für Bildung und Forschung) and the Ministry for Science, Research and Arts Baden-Wuerttemberg (Ministerium für Wissenschaft, Forschung und Kunst Baden-Württemberg), Tech. Rep., Universities of Baden-Württemberg, 2007–2010.